

Original Article

Analysis of Coplanar Capacitive Coupled Wideband Microstrip Antennas

Veeresh G. Kasabegoudar

Associate Professor and Head, Department of Electronics and Communication Engineering, Central University of Karnataka, Kalaburagi, 585367, India.

veereshgk2002@rediffmail.com

Abstract - In this paper, input impedance analysis of rectangular, modified rectangular (one side fractal/staircase shaped), triangular, and semi-elliptical capacitive coupled coplanar microstrip antennas have been presented. The proposed models presented here are for capacitive coupled suspended geometries. These models are developed based on the simple circuit theory approaches, which also include the coaxial feed and capacitively coupled feed strip placed outside the radiator patch. In all cases presented, the calculated results fairly agree with the experimental and simulated data. The proposed models help in finding the input impedance of the capacitively coupled antennas through computer-aided (CAD) models.

Keywords — Capacitive coupling, Input impedance, Semi-Elliptical MSA, ETMSA

I. INTRODUCTION

Microstrip antennas are becoming more and more popular for 5G and recent wireless applications [1-3]. However, finding input impedance is the main concern for proper tuning of the microstrip antenna. Therefore, the input impedance of microstrip antennas is a vital component in finding the exact coupling between antenna terminals and the lines carrying signals to be transmitted and/or received. Several works on finding the input impedances of microstrip antennas have been reported in the literature [4-16]. Some of these works are transmission line model [4], cavity-based approach [5], method of moment solutions [9], and circuit modeling approaches [6, 10-15], etc. However, some of these techniques involve solving complicated integrals and/or require huge memory/time of the computer. However, the works reported by researchers on circuit models [6, 10-20] for the analysis of antenna input characteristics are not only simple to understand and nearly accurate but also provide physical insight into the antenna geometries. In another work, the input impedance analysis of capacitive coupled coaxial probe fed coplanar UWB MSA was reported by [16], which is based on the method of moment's (full wave) analysis. But it is noteworthy that the reported technique requires rigorous calculations for the basic radiator patch. The input impedance calculation using the equivalent circuit approach for the rectangular geometry is reported in [18, 21].

However, these cover only basic rectangular microstrip geometry. In another work, authors of [23] have attempted to model the slit-loaded truncated microstrip antenna based on [21] and [22].

In this paper, the input impedance analysis of capacitively coupled with coaxial-probe fed coplanar wideband microstrip antennas is presented. Almost all models available in the literature assume that the coaxial feed is directly connected to the radiator element. However, the presented model can be used for finding input impedance based on the circuit theory approach, which also includes the coaxial feed placed outside the patch element into the whole model. Further in the literature, input impedance analysis with this type of feed are available for only rectangular geometries. But this paper covers other complicated geometries (modified RMSA, ETMSA, and semi-elliptical MSAs) for input impedance analysis. The developed techniques presented here are easy to evaluate and are best suited for realization with computer-aided design models.

Section II-A includes the analysis of the input characteristics (simulated, measured, and calculated from our model) of basic rectangular geometry [22]. The model developed here is generalized by extending it to find the input impedance of modified rectangular geometry and is covered in subsection II B. Further, input impedance analysis of other shapes of the capacitively coupled antenna (Triangular and Semi-Ellipse) is presented in Section III. Finally, the conclusions of the work presented in this paper are covered in Section IV.

II. BASIC ANTENNA AND ITS IMPEDANCE ANALYSIS

Analysis of the basic rectangular patch antenna is explained in the following subsections.

A. Regular RMSA Geometry

The basic rectangular patch antenna geometry is shown in Fig. 1. The antenna was designed to operate at 5.9 GHz and its optimized dimensions ($L=15.5\text{mm}$, $W=16.4\text{mm}$, $h=1.56\text{mm}$, $d=0.5\text{mm}$, $t=1.2\text{mm}$, $s=3.7\text{mm}$, and $\tan(\delta)=0.0013$, RO3003 Rogers Substrate with $\epsilon_r=3.0$) [22]. The configuration is a microstrip antenna geometry in which the patch and the feed-strip are suspended above the



substrate of height “h” mm. A long-pin probe connector is used to connect the feed strip, which capacitively couples the energy to the main patch. The thorough design procedure of the basic antenna (Fig. 1), parametric studies for the optimization of this geometry, and optimized parameters can be found in earlier works reported by this author [18-22].

To calculate the input impedance of the antenna, the whole geometry is divided into different sections, viz. radiator patch, feed section, and separation between the main patch and a feed strip. These sections can be analyzed individually from well-known circuit theory as explained in [22]. The complete circuit after combining all individual parts is shown in Fig. 2.

$$Z_{in} = \left[\frac{1}{Z_{patch}} + j\omega C_{p1} \right]^{-1} + \frac{1}{j\omega C_s} + \left[\frac{1}{Z_{feed_strip}} + j\omega C_{p2} \right]^{-1} + jX_{probe} \quad (1)$$

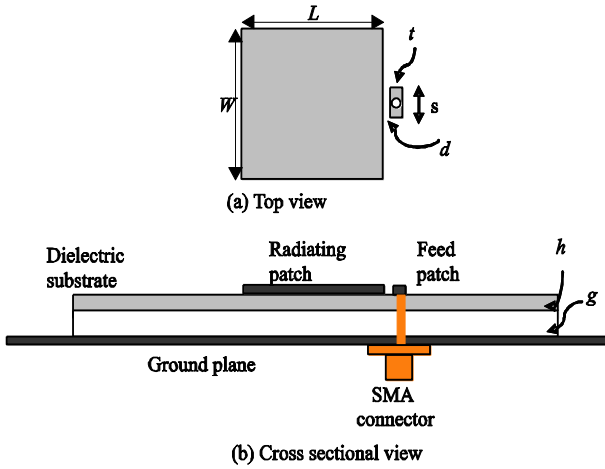


Fig. 1 Geometry of a rectangular patch antenna with a capacitively coupled feed

In (1), Z_{patch} is the input impedance of the equivalent circuit of the patch, and Z_{feed_strip} is the input impedance of the feed strip.

The geometry of the antenna shown in Fig. 1 with optimum parameters ($L=15.5\text{mm}$, $W=16.4\text{mm}$, $h=1.56\text{mm}$, $d=0.5\text{mm}$, $t=1.2\text{mm}$, $s=3.7\text{mm}$, and $\tan(\delta)=0.0013$, RO3003 Rogers Substrate with $\epsilon_r=3.0$) was fabricated, and its input return loss characteristics, gain, and radiation patterns were measured. The input impedance model given by (1) was developed in MATLAB. The S_{11} characteristics obtained from simulation, measurement, and presented model are compared in Fig. 3. It may be noted from Fig. 3 that the developed model values fairly agree with simulated and measured data.

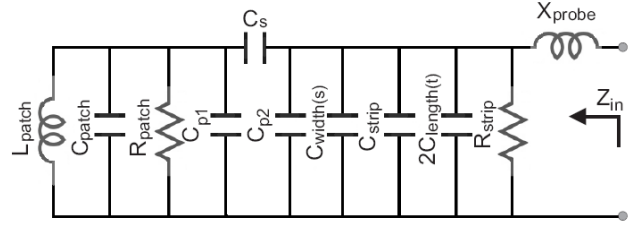


Fig. 2 S_{11} characteristics comparisons of antenna geometry shown in Fig. 1

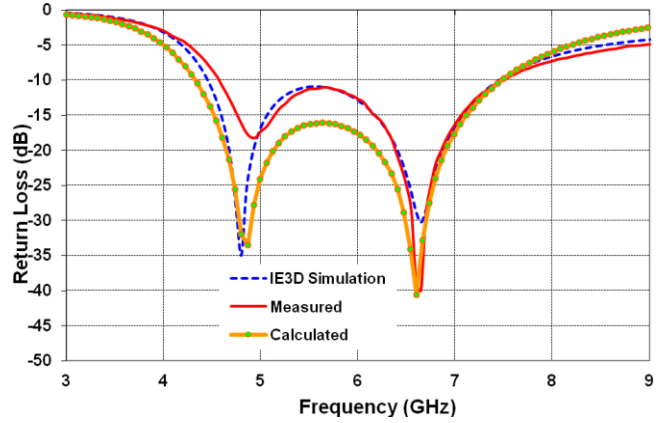
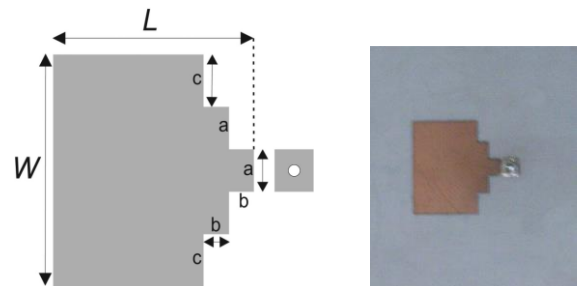


Fig. 3 S_{11} characteristics comparisons of antenna geometry shown in Fig. 1

B. Modified RMSA Geometry

Further to test the design flexibility, the basic model presented in Section II-A has been investigated on the modified rectangular capacitive coupled suspended geometry, as is shown in Fig. 4. The geometry presented here is analyzed as follows. Total geometry is divided into two half parts. The first half is simple rectangular geometry with reduced size by an area covered by staircase shape ($W \times (L-2a)$) sq. mm. And, the second half is the modified area with two rectangles. The first rectangle with an area of $w \times 3a$ sq. mm, and the second rectangle with an area of $an \times b$ sq. mm. Besides this, the discontinuities of the microstrip portions are analyzed using the well-known equivalent circuits shown in Fig. 5 (a) & (b) [24]. Based on this, the modeling of this geometry is presented in the following subsection.



(a) Modified RMSA (b) Fabricated prototype
Fig. 4 Modified RMSA with capacitive feed

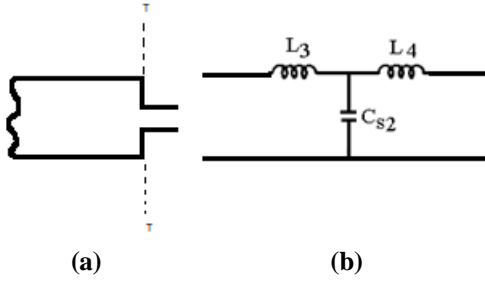


Fig. 5 (a) Step in microstrip width (b) Equivalent circuit

Equations (10) and (11) can be used to calculate the L_1 and L_2 [24]:

$$L_1 = \frac{L_{w1}}{L_{w1} + L_{w2}} L_s \quad (2)$$

$$L_2 = \frac{L_{w2}}{L_{w1} + L_{w2}} L_s \quad (3)$$

Where L_{w1} and L_{w2} can be calculated from (4) and (5)

$$L_{w1} = \frac{Z_{0(w1)} \sqrt{\epsilon_{re(w1)}}}{c} \quad H/m \quad \text{and} \quad (4)$$

$$L_{w2} = \frac{Z_{0(w2)} \sqrt{\epsilon_{re(w2)}}}{c} \quad H/m \quad (5)$$

And, L_s is calculated from the (6) (for <5% error) or from (7) [24]:

$$\frac{L_s}{h} (nH/m) = 40.5 \left(\frac{W_1}{W_2} - 1.0 \right) - 75 \log \left(\frac{W_1}{W_2} \right) + 0.2 \left(\frac{W_1}{W_2} - 1 \right)^2 \quad (6)$$

Or, by using the more general expression:

$$L_s = 0.000987h \left(1 - \frac{Z_{0(w1)}}{Z_{0(w2)}} \sqrt{\frac{\epsilon_{re(w1)}}{\epsilon_{re(w2)}}} \right)^2 (nH) \quad (7)$$

Like L_s , there are two expressions for evaluating the C_s . It may be noted that (8) gives the values with an error of <10%. Equation (9) can be used to calculate the values of C_s .

$$\frac{C_s}{\sqrt{W_1 W_2}} (pF/m) = (10.1 \log \epsilon_r + 2.33) \frac{W_1}{W_2} - 12.6 \log \epsilon_r - 3.17 \quad (8)$$

(for $\epsilon_r \leq 10; 1.5 \leq W_1/W_2 \leq 3.5$)

Or by using (17), which is a more general expression:

$$C_s = 0.00137 \frac{\sqrt{\epsilon_{re(w1)}}}{Z_{0(w1)}} \left(1 - \frac{W_1}{W_2} \right) h \left[\frac{\epsilon_{re(w1)} + 0.3}{\epsilon_{re(w1)} - 0.258} \right] \left[\frac{W_1/h + 0.264}{W_1/h + 0.8} \right] (pF) \quad (9)$$

In this paper, expressions (14) and (16) have been used to find the values of L_s and C_s , respectively, as permittivity and transition width ratios (W_1/W_2) match with the specified range of these values.

The geometry shown in Fig. 4 is analyzed by splitting it into the following parts. The first and second transitions indicated by 1 and 2 in Fig. 4 can be represented by three elements, i.e., L_1 , L_2 , and C_{s1} . These elements can be calculated from the equations given in [26]. Further, as explained earlier, the two plate capacitances of two rectangles, $3a \times b$, and $an \times b$, are

calculated from the standard parallel plate capacitance equations with some necessary modifications for suspended configurations as given in (10) and (11).

$$C_1 = \frac{\epsilon_0 \epsilon_{reff}(3axb)}{(g+h)} \quad (10)$$

$$C_2 = \frac{\epsilon_0 \epsilon_{reff}(axb)}{(g+h)} \quad (11)$$

Finally, the R , L , C elements for the reduced patch with an area of $W \times L-2a$ are calculated. This is the metallic area after subtracting the modified area from the main patch ($W \times L$). This can be modeled as a patch equivalent, i.e., using parallel R_{patch} , L_{patch} , and C_{patch} elements with total length L is replaced by reduced length ($L-2b$). These values may be computed from (12)-(15).

$$C_{patch} = \frac{\epsilon_0 \epsilon_{reff} W(L-2b)}{2(g+h)} \quad (12)$$

$$L_{patch} = \frac{1}{C_{patch} \omega_c^2} \quad (13)$$

$$R_{patch} = \frac{Q_T}{\omega_c C_{patch}} \quad (14)$$

In the end, all these subsections are clubbed to get the final model, which is shown in Fig. 6.

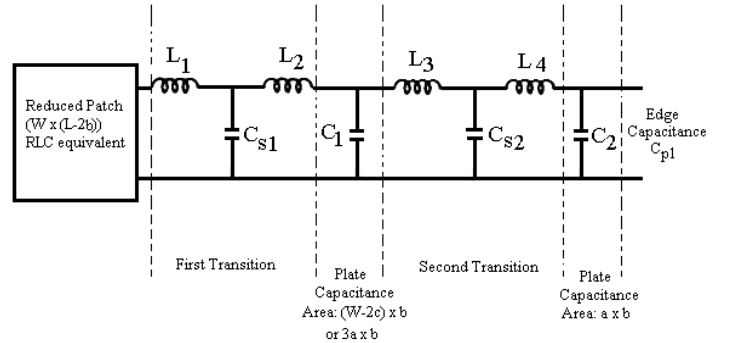


Fig. 6 Derived equivalent circuit for the antenna geometry shown in Fig. 4

The total impedance is calculated by using the circuit theory approach from Fig. 6, which is an equivalent circuit of the geometry shown in Fig. 4 as follows. The reduced patch area's input impedance can be written as:

$$Z_{reduced_patch} = Y_{patch}^{-1} = \left[\frac{1}{R_{patch}} + j \left(\omega C_{patch} - \frac{1}{\omega L_{patch}} \right) \right]^{-1} \quad (15)$$

In (15) C_{patch} , L_{patch} , R_{patch} are as given in (12)-(14). Further, simplifying the circuit shown in Fig. 6 as:

$$Z_A = Z_{reduced_patch} + j\omega L_1 \quad (16)$$

$$Z_B = \left[\frac{1}{Z_A} + j\omega C_{s1} \right]^{-1} \quad (17)$$

$$Z_C = Z_B + j\omega L_2 \quad (18)$$

$$Z_D = \left[\frac{1}{Z_C} + j\omega C_1 \right]^{-1} \quad (19)$$

$$Z_E = Z_D + j\omega L_3 \quad (20)$$

$$Z_F = \left[\frac{1}{Z_E} + j\omega C_{s2} \right]^{-1} \quad (21)$$

$$Z_G = Z_F + j\omega L_4 \quad (22)$$

$$Z_{patch} = \left[\frac{1}{Z_G} + j\omega C_2 \right]^{-1} \quad (23)$$

Where impedance expressions from Z_A to Z_G are cumulative values, feed, section, and coupling between feed-strip and main patch expressions remain the same as that of the basic patch model and all other geometries presented so far. Finally, the total input impedance is calculated using (1). The input characteristics obtained for this geometry are presented in Fig. 7. From Fig. 7 it may be noted that the modeled S_{11} curve closely follows the simulated curve except S_{11} depth mismatch at first resonance. However, the depth of S_{11} does not make sense when it is already below -10dB.

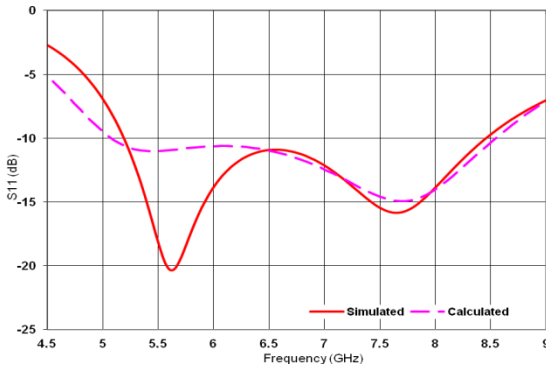


Fig. 7 S_{11} characteristics comparison of modified RMSA antenna geometry

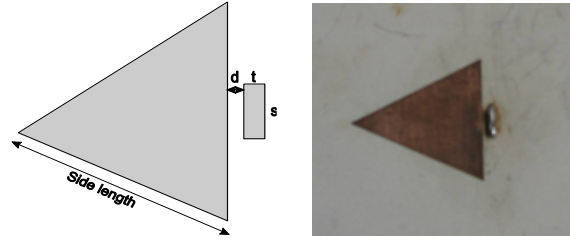
III. INPUT IMPEDANCE OF OTHER GEOMETRIES

The model obtained in Section II has been further investigated for triangular and semi-ellipse geometries. Triangular and semi-ellipse geometries equivalent circuit elements are calculated by equating the area of these geometries to circular microstrip and are discussed in the following subsections. Once the equivalent elements of these geometries are computed, these values can be used to find the input impedance using the main equation (1). Analysis of all these geometries has been presented in the following subsections.

A. Equilateral Triangular Microstrip Antenna (ETMSA)

The antenna geometry used for simulation and analysis is shown in Fig. 8. The triangular patch was designed to operate for the same resonant frequency (5.9GHz) and has the dimensions of base=19.75mm and height=17.1mm, and then it was optimized for maximum impedance bandwidth

using the key design parameters (separation between the main antenna element and feed strip (d) = 0.5mm, and feed strip dimensions $t=2.0$ mm and $s=4.5$ mm). The feed is located parallel to the base, as shown in Fig. 8. The total capacitance (parallel plate and fringing) of ETMSA can be found by equating its area with the rectangular/circular microstrip geometry.



(a) ETMSA geometry (b) Prototype
Fig. 8 Geometry of an equilateral triangular microstrip antenna (ETMSA)

Equation (24) represents the ETMSA's total capacitance which is obtained from the circular microstrip disc capacitance by replacing 'a' with ' a_{eq} ' [25].

$$C_T = \frac{a_{eq} \pi \epsilon_r \epsilon_0}{h} \left[1 + \frac{2h}{a_{eq} \pi \epsilon_r} \left\{ \ln \left(\frac{a_{eq}}{2h} \right) + (1.41 \epsilon_r + 1.77) + \frac{h}{a_{eq}} (0.268 \epsilon_r + 1.65) \right\} \right] \quad (24)$$

In Equation (24), ' a_{eq} ' is given by

$$a_{eq} = \sqrt{\frac{A_{triangle}}{\pi}} \quad (25)$$

In (25), ' $A_{triangle}$ ' represents the area of the original triangle.

From (26), the parallel plate capacitance and the fringing capacitances can be written after necessary air-dielectric medium corrections as:

$$C_{patch} = \frac{a_{eq}^2 \pi \epsilon_{reff} \epsilon_0}{(g+h)} \quad (26)$$

$$C_{p1} = C_{patch} \left[\frac{2(g+h)}{a_{eq} \pi \epsilon_{reff}} \left\{ \ln \left(\frac{a_{eq}}{2(g+h)} \right) + (1.41 \epsilon_{reff} + 1.77) + \frac{(g+h)}{a_{eq}} (0.268 \epsilon_{reff} + 1.65) \right\} \right] \quad (27)$$

Equation (26) can be used in place of rectangular patch capacitance (C_{patch} shown in Fig. 2), and (27) can be used to calculate one of the parallel capacitors (C_{p1}). Other elements of Fig. 2 can be calculated as explained in [19-22]. The S_{11} characteristics obtained for the triangular microstrip patch antenna are shown in Fig. 9. From Fig. 9, it can be noticed that there is a proper matching between the simulated and calculated results in the band of operation (-10dB bandwidth range).

B. Semi-elliptical Microstrip Patch Antenna

The geometry of semi-elliptical microstrip patch antenna is shown in Fig. 10. The semi-elliptical microstrip antenna was designed for the best possible bandwidth

(4.1GHz to 6.6GHz = 2.5GHz) as suggested in [26] with the dimensions indicated in Fig. 10 ($a=19\text{mm}$, $b=8.23\text{mm}$, $d=0.5\text{mm}$, $s=4.5\text{mm}$ and $t=1.6\text{mm}$). The total capacitance of the semi-ellipse can be calculated by considering the complete elliptical geometry and then taking half the total capacitance to represent the semi-ellipse. An aperture dimension of a semi-elliptical patch is calculated by considering an equivalent circular patch having the same “metal area”. Therefore the semi-elliptical area is calculated by considering two circles of radii ‘ a ’ and ‘ b ’ as suggested in [26] for the elliptical patch. It should be noted that in Fig. 10 ‘ a ’ and ‘ b ’ are the semi-major and semi-minor axes of ellipse geometry.

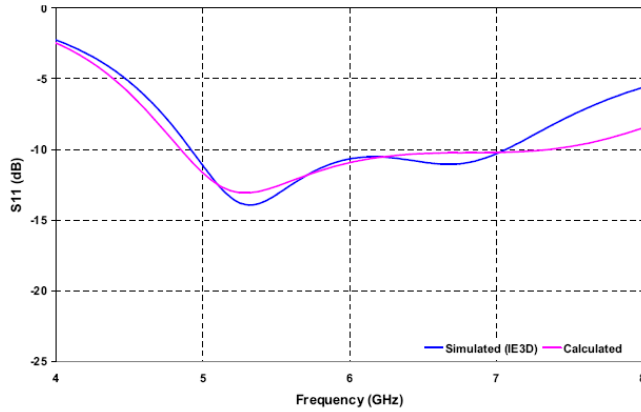
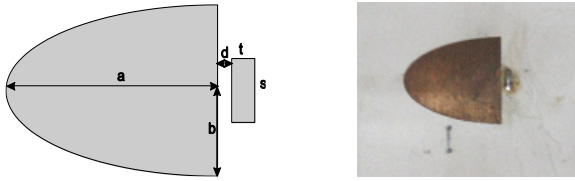


Fig. 9 S₁₁ characteristics comparison of ETMSA



(a) Ellipse geometry (b) Prototype
Fig. 10 Geometry of semi-elliptical microstrip antenna

$$A_{\text{semi-ellipse}} = 0.5\sqrt{A_{\text{circle1}} \times A_{\text{circle2}}} = \frac{\pi}{2} ab \quad (28)$$

With the fringing fields included, it can be written as

$$A_{\text{semi-ellipse}} = \frac{\pi}{2} a_{\text{eq}} b_{\text{eq}} \quad (29)$$

Where

$$a_{\text{eq}} = \left[a^2 + \frac{2ah}{\pi\epsilon_{\text{reff}}} \left\{ \ln\left(\frac{a}{2h}\right) + (1.41\epsilon_{\text{reff}} + 1.77) + \frac{h}{a}(0.268\epsilon_{\text{reff}} + 1.65) \right\} \right]^{\frac{1}{2}} \quad (30)$$

Similarly, b_{eq} can be calculated by replacing the term ‘ a ’ in (30) with ‘ b ’. Therefore, the total capacitance for the elliptical patch is written as:

$$C_T = \frac{\epsilon_0 \epsilon_r \pi a_{\text{eq}} b_{\text{eq}}}{2(g+h)} \quad (31)$$

Similar to the previous case (triangular patch), (31) can be used to write the patch and fringing capacitances separately,

and also complex air-dielectric corrections have to be made before calculation. Like the above two cases (rectangular and triangular patch geometries), here also the calculated and simulated S₁₁ characteristics are closely matching and are depicted in Fig. 11.

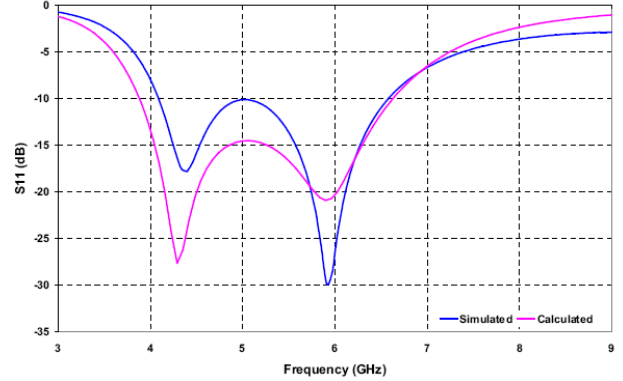


Fig. 11 S₁₁ characteristics comparison for semi-ellipse geometry

IV. CONCLUSIONS

The model developed based on the equivalent circuit theory approach to find the input impedance has been presented. The models proposed here are suitable for evaluating the antenna’s input impedance, including the effects of the feed strip and the probe pin, which are located outside the main radiating element, over an operating bandwidth. Return loss values evaluated using the proposed models fairly match with the simulated and experimental results. Further, the concept has been extended to a modified rectangular microstrip antenna (one side staircase shaped rectangular patch). Here the model equations are derived from the equivalent circuits available for microstrip discontinuities with necessary modifications for suspended geometries. Further, the model developed for rectangular microstrip patch antenna can be extended to all regular microstrip geometries by equating their area with RMSA. Like RMSA, the calculated input return loss characteristics (S₁₁) Triangular and Semi-ellipse were also found to be in good agreement with the simulated results. For these two geometries, also good results have been obtained like other cases demonstrated.

REFERENCES

- [1] Nikita Kothari, Aman Saraf, Manoj Singh Rawat, Design of Compact Coaxial-Fed Meander Slot Multiband Antenna for Wireless Applications, International Journal of Engineering Trends and Technology, 58(1) (2018) 20-24.
- [2] Fath Elrahman I. Khalifa, Ahmed A. Ibrahim, Mamdouh Z. Ibrahim, Mohamed M. Fathalrahman, Muayad A. Alhassan, Design of Dual-band Microstrip Antenna with U-shaped slot, International Journal of Engineering Trends and Technology, 55(1) (2018) 35-40.
- [3] Rhea Nath, Pramod Singh, Designing and Analysis of MIMO Antenna for UWB Applications, International Journal of Engineering Trends and Technology, 56(1) (2018) 25-30.

- [4] A.K. Bhattacharjee, S.R.B. Chaudhuri, A. Mukherjee, D.R. Poddar, and S.K. Chowdhury, Input impedance of rectangular microstrip antennas, *IEE Proc Pt. H.* 135(5) (1988) 351-352.
- [5] Y.T. Lo, D. Solomon, and W.F. Richards, Theory and experiment on microstrip antennas, *IEEE Trans. Antennas Propagat.*, 27(2) (1979) 137-145.
- [6] A. L. Buzov, M. A. Buzova, D. V. Mishin, and A. M. Neshcheret, Calculating the input impedance of a microstrip antenna with a substrate of a chiral metamaterial, *Journal of Communications Technology Electronics Letters*, 63 (2018) 1259-1264.
- [7] D. F. Mona, E. S. Sakomura, and D. C. Nascimento, Circularly polarizing rectangular microstrip antenna design with arbitrary input impedance, *IET Microwaves, Antennas and Propagation*, 12(9) (2018) 1532-1540.
- [8] A. A. Baba, M. A. Zakariya1, Z. Baharudin, M. Z. U. Rehman, M. F. Ain, and Z. A. Ahmad, Equivalent lumped-element circuit of aperture and mutually coupled cylindrical dielectric resonator antenna array, *Progress in Electromagnetic Research C*, 45 (2013) 15-31.
- [9] S. Singhal, Ultra-wideband elliptical microstrip antenna for terra-Hertz applications, *Microw. Opt. Technol. Lett.*, 61(10) (2019) 2366-2373.
- [10] A. Majumdar, S. K. Das, and A. Das, Ultra-wideband CPW fed patch antenna with fractal elements and DGS for wireless applications, *Progress in Electromagnetic Research C*, 94 (2019) 131-144.
- [11] E.H. Newman and T. Pravit, Analysis of microstrip antennas using moment methods, *IEEE Trans. Antennas Propagat.*, 29(1) (1981) 47-53.
- [12] M. P. Joshi and V. J. Gond, Design and analysis of microstrip patch antenna for WLAN and vehicular applications, *Progress in Electromagnetic Research C*, 97(2019) 163-176.
- [13] J.P. Damiano, J. Bennegouche, and A. Papiernik, Study of multilayer microstrip antennas with radiating elements of various geometries, *IEE Proc Pt. H.* 137(3) (1990) 163-170.
- [14] J.P. Damiano and A. Papiernik, Survey of analytical and numerical models for probe-fed microstrip antennas, *IEE Proc. Microw. Antennas Propagat.*, 141(1) (1994) 15-22.
- [15] V.K. Pandey and B.R. Vishvakarma, Analysis of an E-shaped patch antenna, *Microw. Opt. Technol. Lett.*, 49(1) (2007) 4-7.
- [16] J.A. Ansari and R.B. Ram, Analysis of a compact and broadband microstrip patch antenna, *Microw. Opt. Technol. Lett.*, 50(8) (2008) 2059-2063.
- [17] A.K. Verma, N.V. Tyagi, and D. Chakraverty, Input impedance of probe fed multilayer rectangular microstrip patch antenna using the modified Wolff model, *Microw. Opt. Technol. Lett.*, 31(3) (2001) 237-239.
- [18] G. Mayhew-Ridgers, J.W. Odendaal, and J. Joubert, Efficient full-wave modeling of patch antenna arrays with new single-layer capacitive feed probes, *IEEE Trans. Antennas Propagation*, 53(2005) 3219-3228.
- [19] V.G. Kasabegoudar, D.S. Upadhyay, and K.J. Vinoy, Design studies of ultra-wideband microstrip antennas with a small capacitive feed, *Int. J. Antennas Propagat.*, (2007) 1-8.
- [20] V.G. Kasabegoudar and K.J. Vinoy, A wideband microstrip antenna with symmetric radiation patterns, *Microw. Opt. Technol. Lett.*, 50(8) (2008) 1991-1995.
- [21] V. G. Kasabegoudar, Low profile suspended microstrip antennas for wideband applications. *J. Electromagn. Waves Appl.* 25(2011) 1795–1806.
- [22] V.G. Kasabegoudar and K.J. Vinoy, A wideband microstrip antenna with symmetric radiation patterns, *IEEE Trans. Antennas Propagat.*, 58(10) (2010) 3131-3138.
- [23] D. K. Singh, B. K. Kanujia, S. Dwari, and G. P. Pandey, Modeling of a dual circularly polarized capacitive-coupled slit loaded truncated microstrip antenna, *Journal of Computational Electronics*, 19(4) (2020) 1564-1572.
- [24] K.C. Gupta, R. Garg, I. bahl, and P. Bhartia *Microstrip Lines and Slotlines*, 2nd Edition, Artech House, London, (1996).
- [25] W. C. Chew and J. A. Kong, Effects of fringing fields on the capacitance of circular microstrip disc, *IEEE Trans. Microw. Theo. Tech.*, 28(2) (1980) 98-104.
- [26] P. Mythili and A. Das, Simple approach to determine resonant frequencies of microstrip antennas, *IEE Proc.-Microw. Antennas Propagat.*, 45(2) (1998) 159-162.